Title
Engineering chemically modified viruses for prostate cancer cell recognition

Journal
Molecular Omics, 11(12)

ISSN
2515-4184

Authors
Mohan, K
Weiss, GA

Publication Date
2015-12-01

DOI
10.1039/c5mb00511f

Molecular BioSystems

PAPER

View Article Online
View Journal | View Issue

Cite this: *Mol. BioSyst.*, 2015, **11**, 3264

Engineering chemically modified viruses for prostate cancer cell recognition†

K. Mohan[a] and G. A. Weiss*[ab]

Received 30th July 2015,
Accepted 7th October 2015

DOI: 10.1039/c5mb00511f

www.rsc.org/molecularbiosystems

Specific detection of circulating tumor cells and characterization of their aggressiveness could improve cancer diagnostics and treatment. Metastasis results from such tumor cells, and causes the majority of cancer deaths. Chemically modified viruses could provide an inexpensive and efficient approach to detect tumor cells and quantitate their cell surface biomarkers. However, non-specific adhesion between the cell surface receptors and the virus surface presents a challenge. This report describes wrapping the virus surface with different PEG architectures, including as fusions to oligolysine, linkers, spacers and scaffolded ligands. The reported PEG wrappers can reduce by >75% the non-specific adhesion of phage to cell surfaces. Dynamic light scattering verified the non-covalent attachment by the reported wrappers as increased sizes of the virus particles. Further modifications resulted in specific detection of prostate cancer cells expressing PSMA, a key prostate cancer biomarker. The approach allowed quantification of PSMA levels on the cell surface, and could distinguish more aggressive forms of the disease.

Introduction

The migration and dissemination of tumor cells, termed metastasis, causes ≈90% of cancer deaths.[1,2] Metastasis requires loss of apoptotic regulation, and such cells respond poorly to conventional anti-cancer treatments. With a majority of the estimated 27 540 deaths from prostate cancer (PCa) in the US for 2015[3] resulting from metastasis,[2] new methods for efficient detection and characterization of metastatic cells could impact clinical care and patient prognosis. Previously, we reported the sensitive detection of soluble prostate-specific membrane antigen (PSMA), a PCa biomarker, at 100 pM concentrations using viruses incorporated into an electrically conductive polymer.[4] Here, we engineer similar bacteriophage, termed 'phage,' with polymers and ligands for direct binding to PSMA found on the surface of PCa cells.

PSMA, a 750 residue, 90 kD glycoprotein, is overexpressed on the surface of tumor cells as a non-covalent homodimer in both primary and metastatic cancers.[5,6] Differential splicing during tumorigenesis leads to expression of PSMA as a type II integral membrane protein.[7] Elevated PSMA levels have also been observed in seminal fluid and urine of PCa patients.[8] To detect the protein in urine, we reported viruses with both genetically encoded and chemically synthesized ligands for the sensitive detection of PSMA.[4,9] These ligands, selected from phage-displayed peptide libraries had the following amino acid sequences: ligand-**1** (CALCEFLG) and ligand-**2** (SECVEVFQNSCDW). Genetically encoded, phage-displayed ligand-**2** binds with >100-fold higher affinity to PSMA than ligand-**1**.[4,10]

Used ubiquitously for molecular display applications, the M13 filamentous phage applied here infects *E. coli*, and can be manipulated to present genetically encoded peptides on the phage surface.[11–13] The M13 virus consists of a circular, single-stranded DNA genome surrounded by a protein coat composed of approximately 2700 copies of the major coat protein, P8, an α-helical protein of 50 amino acid residues with an unstructured N-terminus. One Glu and two Asp residues near the N-terminus of P8 impart a high negative charge to the outer surface of the virus at physiological pH.[14] Selections with phage-displayed libraries of peptides and proteins can target tissue-cultured cells and even organs in living organisms.[15–19] Phage have also been incorporated into nanomedicine platforms for targeted drug delivery[20–24] and imaging.[25,26] Such applications require low background binding by phage to cell surfaces.

Phage typically adhere to cell surfaces with high affinity, however. Such non-specific adhesion complicates the design of phage-based sensors for the detection of tumor cells; the non-specific background can reduce the signal to noise ratios and the ability to distinguish tumor from non-tumor cells. Francis and co-authors have reported covalently linking the coat proteins of fd phage with both polyethylene glycol (PEG) and imaging

[a] *Department of Chemistry, University of California, Irvine, 1102 Natural Sciences 2, Irvine, California 92697-2025, USA*
[b] *Department of Molecular Biology and Biochemistry, University of California, Irvine, 1102 Natural Sciences 2, Irvine, California 92697-2025, USA.*
E-mail: gweiss@uci.edu

† Electronic supplementary information (ESI) available: Materials and methods, references, and thirteen supplementary figures. See DOI: 10.1039/c5mb00511f

agents through a two step reaction.[27] M13 and fd phage are closely homologous with similar sizes, structural features and sequences.[28] An alternative approach described here, applies non-covalent attachment to the phage surface to access additional architectures for biosensor applications.

Non-covalent attachment offers comparable stability to covalent modification of the virus surface. The high negative charge on the phage surface allows non-covalent wrapping with cationic peptides and polymers.[29,30] Linking these wrappers to recognition ligands opens new routes to greater sensitivity and specificity for target analytes. The peptide ligands can be chemically synthesized and fused to an oligolysine peptide (K_{14}), which 'wraps' around the virus particle through complementary electrostatic interactions. Previously, this strategy allowed maximization of ligand density on the phage surface for sensitive detection of biomarkers in complex biofluids, such as synthetic urine.[4] Here, the overall design incorporates PEG polymers in conjunction with this wrapping strategy to address the problem of non-specific adhesion between phage and cells. Then, we optimize various architectures for the specific detection of PCa cells.

Results and discussion

Non-specific adhesion of viruses to cells

Among prostate cancer cell lines, LNCaP cells provide the most commonly used *in vitro* model for early stage PCa.[31,32] Derived from the lymph node adenocarcinoma of the human prostate, LNCaP expresses most of the important PCa biomarkers including PSMA, PSA and AR.[33] Attempts to recognize cell surfaces with conventional phage-displayed ligands resulted in unacceptably high, non-specific adhesion by control phage, which lack a displayed peptide. As shown by ELISA, phage-displayed PSMA ligand **2** and control phage produced similar high levels of binding to LNCaP cells (Fig. S1, ESI†). In this and essentially all ELISAs reported here, cells are immobilized on microtiter plates; phage are then added before washing away non-binding viruses, and levels of bound phage are quantified spectrophotometrically using an anti-M13 antibody conjugated to horse radish peroxidase (HRP), which catalyzes conversion of its substrate into a colored product. Thus, the high levels of adhesion by both ligand-displayed and control phage are due to non-specific adhesion between phage coat proteins and abundant cell surface receptors, glycans and other molecules. To overcome this non-specific adhesion, we focused on eliminating such interactions by control phage.

Wrapping phage with PEG to prevent non-specific adhesion

The water soluble polymer PEG is commonly bioconjugated to proteins to reduce non-specific adhesion to cells and other surfaces.[34–37] In addition, PEG can increase the solubility of attached therapeutic proteins, prolong circulation times, and decrease proteolysis.[38] Furthermore, the activities of proteins conjugated to PEG typically remain unaffected.[39,40] PEG has been shown to broadly adopt two distinct conformations – descriptively termed 'mushroom' and 'brush'.[34,41,42] The transition from the mushroom conformation, a more random orientation, to the brush conformation is dependent upon the polymer length and packing densities; longer PEG lengths and higher packing densities favor formation of the brush conformation. This transition can result in a significant drop in non-specific adsorption. In many systems, a mole fraction of 0.15 PEG-modified to -unmodified sites yields significantly reduced non-specific adhesion. High packing densities with such mole fractions can force the polymer to adopt a more stretched, and extended brush conformation to more effectively suppress non-specific adhesion.[34] To provide a framework for experimental design and data interpretation, the reported PEG polymers are assumed to form mushroom and brush conformations based on PEG lengths and packing densities, as has been reported previously.[34,41,42]

Initial attempts to block non-specific cell adhesion applied PEG variants with different MWs as phage wrappers. Azide-functionalized, polydispersed PEGs with size distributions centered around 7, 22 or 45 ethylene glycol units (providing average MWs of 300, 1k or 2k, respectively) were conjugated to K_{14}-alkyne using the Cu^{I}-catalyzed cycloaddition ('click') reaction, Fig. S2–S4 (ESI†). The conjugated peptides were then purified by reverse-phase HPLC and characterized by MALDI-TOF mass spectrometry. The relative adhesion levels of unwrapped and PEG-wrapped phage targeting immobilized LNCaP cells were compared by phage-based ELISA, Fig. S5 (ESI†). Since the phage lacked a displayed peptide, adhesion could only result from non-specific interactions by the phage coat proteins.

In theory, phage wrapped with PEG should bind to LNCaP cells with much lower affinity due to decreased non-specific adhesion. However, no such reduction was observed for the different MW PEGs used, Fig. S5 (ESI†). The ineffectiveness of this initial approach likely resulted from interaction between PEG and the K_{14} sidechains used to wrap the phage. A crown ether-like encapsulation can form between the primary amine of the Lys sidechains and ethylene glycols of PEG,[43] thereby rendering K_{14} incapable of wrapping the phage surface. Without the PEG wrapping the phage surface, the results merely compare phage in different assay wells, as is evident from the overlapping responses. The lack of wrapping by PEGylated oligolysine was further verified by dynamic light scattering measurements, which revealed no significant change in the cross-sectional diameter of the treated phage (data not shown).

On-phage cycloaddition reaction to generate PEGylated phage

To overcome K_{14} encapsulation by PEG, phage with PEG wrappers were generated in two steps, Fig. 1. First, phage were wrapped with K_{14}-alkyne by incubation at room temperature for 15 min. During this step, the K_{14}-alkyne wrap the phage prior to PEG conjugation. Next, PEG azides were added, and the cycloaddition reaction with the K_{14}-alkyne took place on the phage surface for 30 min. Next, the ELISA described for Fig. S5 (ESI†) was repeated with these PEGylated phage comparing the non-specific adhesion of phage wrapped with different MW PEGs, Fig. 2; in this experiment negative controls of 'No wrap' and 'No cells' indicate the extremes of high levels

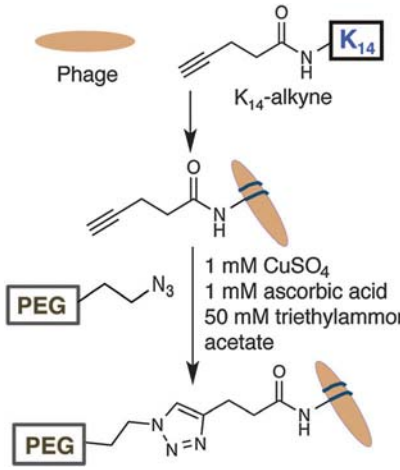

Fig. 1 Schematic illustration of the on-phage cycloaddition reaction to bioconjugate PEG polymers to the phage surface. Phage are first wrapped with K_{14}-alkyne, and then conjugated to different lengths of azide-functionalized PEG polymers.

of non-specific adhesion to LNCaP cells and non-binding, respectively. Phage wrapped with PEG45 and PEG100 (average MW 2k and 5k, respectively) demonstrate a >75% reduction in non-specific binding to LNCaP cells, as demonstrated by the observed decrease in HRP activity resulting from lower phage binding. The experiment confirms that PEG wrappers can effectively suppress non-specific adhesion, provided the K_{14} wraps around the phage first. The reduction in non-specificity increases with larger MW PEG polymers, and saturates at around 45 ethylene glycol units.

PEG reduces non-specific binding largely by surrounding the attached surface with a hydration sphere.[44] Direct contact to the phage surface, termed primary adsorption, requires smaller non-specific binding partners to penetrate the PEG layer. Alternatively, the non-specific binding partners could adhere to the outer surface of the PEG layer, termed secondary adsorption. For non-specific adhesion to the larger surfaces of cells, such secondary adsorption is likely a more pronounced effect. To minimize secondary adsorption, the wrappers were applied at 0.15 mole fraction.[34] Here, we estimate the mole fraction as the stoichiometry of PEG molecules added to P8 coat proteins; this analysis is analogous to the calculations for PEG grafted in lipid membranes.[45] Additionally, we assumed that at the concentration used, PEG22, 45 and 100 adopt brush conformations due to their high packing densities,[34,41] which were fixed by maximization of oligolysine wrappers as previously described.[4]

Based on published precedent, PEG7 presumably adopts a mushroom conformation,[34] and fails to suppress non-specific adhesion to the same levels. The brush conformation of the larger PEGs can more efficiently reduce non-specific secondary adsorption due to the hydration sphere extending further from the virus surface. Beyond a certain height of the polymer brush, the effect of secondary adsorption remains constant as shown by the nominal difference obtained between PEG45 and 100 in Fig. 2. For ligand-based recognition described further below, phage wrapped with PEG45 provided the negative control phage.

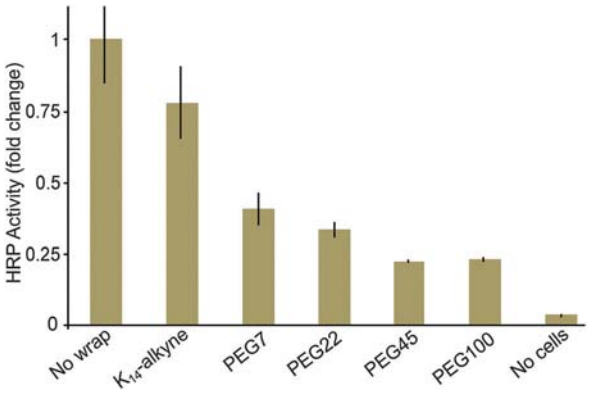

Fig. 2 Phage-based ELISA demonstrating the effectiveness of wrapping phage by click chemistry with the indicated PEG azides to reduce non-specific adhesion to cellular surfaces. A >75% reduction in non-specific adhesion to LNCaP cells is observed for PEG45 compared to unwrapped phage. A lower HRP signal indicates decreased non-specific adhesion. Throughout this report, LNCaP cells are targeted at 4.5×10^6 cells per mL, and error bars for ELISA data represent standard error (n = 3). All experimental data points include such error bars, though often these are quite small. The p-value is <0.01 for all data reported here.

Dynamic light scattering (DLS) analysis of PEGylation

To characterize the PEG-wrapped phage, DLS measurements were conducted, Fig. 3. The M13 phage used here have dimensions of approximately 6 by 1000 nm.[46] Rayleigh scattering provides an estimated 45.9 nm diameter of the average cross-section; this experiment uses measurement with backscatter mode, having a scattering angle of 173°, for unwrapped and unmodified phage. For comparison, the comparable reported measurement with covalently and genetically modified fd phage yielded a reported average cross-sectional diameter of 70 nm.[47] Due to the filamentous nature of the phage as a long, flexible cylinder, such values can only provide a relative change in size. Furthermore, the forward scatter mode (scattering angle of 13°) provides a 715 nm average size for the M13 phage applied here,

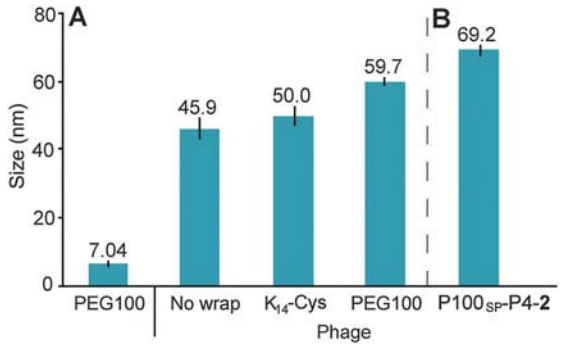

Fig. 3 Dynamic light scattering measurements indicate the consistent increase in size with the addition of wrappers on phage. Labels indicate the measured average size in nm for each indicated sample. Error bars represent standard error (n = 3), with each individual size measurement being the average of ten runs.

which compares well with previously reported 650 nm average size for fd phage.[47] Since the phage length remains roughly unchanged with wrapping, we found negligible difference in the average phage sizes measured by forward scattering, and instead focused on DLS measurement in backscatter mode.

Next, the change in average cross-sectional diameter was measured for different samples from each step of the phage wrapping process, Fig. 3A. The addition of K_{14}-Cys wrappers on the phage leads to an increase in cross-sectional diameter from 45.9 to 50.0 nm. Upon conjugation of this K_{14}-Cys wrapped phage to maleimide-functionalized PEG100, an approximate 10 nm increase in size is observed. This increase in size matches two independent reports for size increases after PEG100 bioconjugation to gold nanoparticles.[48,49] Thus, the DLS-based size measurements confirm the formation of the expected phage-wrapped complexes.

Synthesis of PEGylated ligands

Towards the goal of specific recognition of a cell surface receptor, different scaffolds for the display of ligands on phage were explored. First, heterobifunctional PEG, Mal-PEG-NH_2, provided reactive groups for selective attachment of oligolysine at the maleimide end and PSMA binding ligands to the amine end, Scheme 1. As the scaffold, PEG100 was chosen to provide a longer polymer brush to reduce non-specific secondary adsorption. Azide-functionalized PSMA ligands **1** and **2** were synthesized by conventional solid-phase peptide synthesis (SPPS), and coupled to pentynoic acid *via* the click reaction. The resultant N-terminal carboxylic acid group was then coupled to Mal-PEG100-NH_2 using HBTU as an amide bond forming agent in water. Since this reaction non-specifically couples amine and carboxylate functionalities, the attachment sites could vary as both ligands have sidechain carboxylic acids. The resultant ligand is termed $P100_{NSP}$-**1/2** for 'PEG100, non-specific attachment to ligand **1** or **2**.' as described in Table 1.

Subsequently, phage wrapped with K_{14}-Cys were coupled to the maleimide terminus of $P100_{NSP}$-**1/2**, as described above.

Table 1 Nomenclature of PEGylated PSMA ligands. All ligands were bioconjugated to phage wrapped with K_{14}-Cys

PEG length	Attachment	PEG4 linker	Nomenclature
P100	NSP	—	$P100_{NSP}$-**X**
P100	SP	—	$P100_{SP}$-**X**
P100	NSP	✓	$P100_{NSP}$-P4-**X**
P100	SP	✓	$P100_{SP}$-P4-**X**

SP: specific; NSP: non-specific. **X** = ligand **1** (CALCEFLG) or **2** (SECVEVFQNSCDW).

Preliminary validation of binding to cell surface PSMA by the PEGylated ligand wrappers was performed by phage ELISA as before, Fig. S6 (ESI†). Compared to the non-specific binding observed in Fig. S1 (ESI†), a slight improvement in binding affinity resulted from wrapping with the PEGylated ligands. This modest result provided a starting point for further engineering. Phage wrapped with $P100_{NSP}$-**2** displayed a higher affinity for LNCaP cells compared to $P100_{NSP}$-**1** as expected from its higher binding affinity for PSMA.

Bidentate binding mode of PEGylated ligands

Dual display of ligands **1** and **2** can enable synergistic, high affinity binding to PSMA due to a bidentate binding mode and a velcro-like avidity effect.[4] A phage ELISA targeting LNCaP cells with different ratios of the two PEGylated, phage-wrapped ligands examined relative binding affinities. First, the effectiveness of the bidentate binding mode (red in Fig. 4) was compared to binding by individual ligands (patterned red bars in Fig. 4). Having two ligands on the phage surface consistently improved binding affinity. Furthermore, a 2 : 1 mixture of $P100_{NSP}$-**2** and $P100_{NSP}$-**1** respectively, was found to maximize the recognition of PSMA on LNCaP cells. The improved binding from a 2 : 1 ratio stems from the higher binding affinity of ligand **2** compared to ligand **1**. Altering this ratio in either direction drops the apparent affinity, likely due to loss of optimal bidentate binding. Hereafter, phage

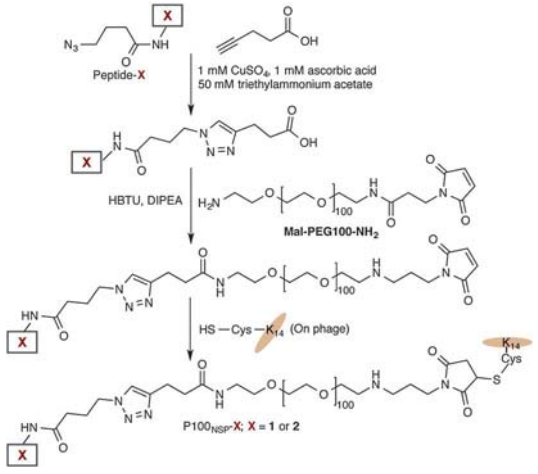

Scheme 1 Synthesis scheme for the generation of PEGylated ligands on phage for the selective detection of PSMA on LNCaP cells. **X** indicates the PSMA binding ligands **1** or **2**.

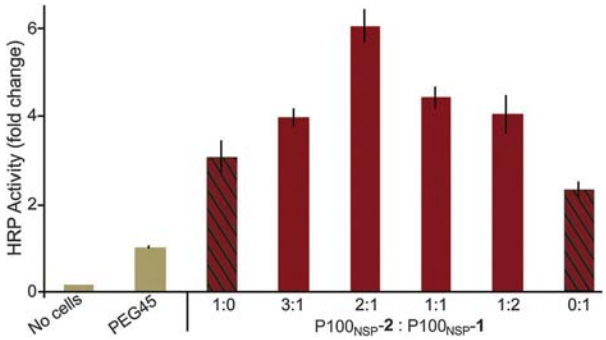

Fig. 4 Phage-based ELISA demonstrating the effectiveness of the bidentate binding mode for the two PSMA binding ligands on the phage surface. A higher HRP activity indicates stronger binding affinity between the displayed ligands and PSMA on the cell surface. The various ratios of wrapped ligands (red bars) can be compared with wrapping by individual ligands (patterned red bars). A 1 : 1 ratio of the two ligands indicates the assay of equimolar amounts of each ligand. Negative controls (gold bars) were as previously described. The p-value is <0.01 for all data reported here.

were wrapped with a 2 : 1 mixture of the PEGylated ligands **2** and **1**, respectively.

Optimizing the attachment site for PEGylated ligands

Further optimization explored the size, geometry and attachment site of the ligands fused to the PEG wrapper. Such variables can be crucial to the pharmacokinetic properties of PEGylated drugs, which demonstrates the sensitivity of biological recognition to such factors.[50] For example, the attachment sites of the peptide ligand to PEG100 dictates the ligand orientation and the potential availability of peptide sidechains. An alternative synthesis scheme was designed to control ligand orientation. Mal-PEG100-NH_2 was first coupled to pentynoic acid, Fig. S7 (ESI†). The resultant Mal-PEG100-alkyne was then coupled to the azide-functionalized peptide ligands using click chemistry, providing a specific site of attachment to the ligand. The resulting PEGylated ligand is termed $P100_{SP}$-**1**/**2** for 'PEG100, specific attachment to ligand **1** or **2**,' as described in Table 1.

Specific attachment of PEG to the wrapped ligands could improve binding affinity by removing attachment through the ligands' sidechains and also altering their orientation on the phage surface. The significance of ligand orientation is apparent through the higher binding affinity observed for genetically encoded, phage-displayed ligand **2** (dashed red line) relative to phage wrapped with chemically synthesized ligand **2** (solid red line), Fig. S8 (ESI†). When genetically displayed on the phage, ligand **2** has a free N-terminus, but the synthesis of $P100_{SP}$-**2** inverts this orientation, leaving a free C-terminus, and an N-terminus directly conjugated to the triazole and then PEG100 (as shown in the schematic flowchart of Fig. S9, ESI†). As attained by the specific attachment of $P100_{SP}$-**2**, the N-terminal Glu residue of ligand **2** requires an unhindered and unmodified carboxylate sidechain, as previously shown by homolog shotgun scanning.[10] The sidechain of Glu2 could be partially modified in $P100_{NSP}$-**2** due to non-specific attachment through the carboxylate sidechain. Subsequent experiments compared bioconjugation to either the N-terminal azide or carboxylate sidechain through incorporation of an additional linker.

Insertion of a PEG4 linker to reduce steric effects on the attached ligands

Heterobifunctional linkers between PEG and a molecule of interest can enhance activity through flexible additional spacing.[44] We envisioned the incorporation of an average 175 MW PEG4 linker between the peptide ligand and the triazole generated by the click reaction could enhance the binding affinity of the peptide ligands. With only four ethylene glycol units, this highly flexible linker can disconnect the peptide ligand from any steric constraints dictated by PEG100 or the triazole, Fig. S9 (ESI†). Thus, the peptide ligands were resynthesized *via* SPPS, and coupled to azido-PEG4-carboxylic acid (15-azido-4,7,10,13-tetraoxapentadecanoic acid), thereby inserting a PEG4 linker before the azide functionality. Azido-PEG4-ligands were further linked to PEG100 following the two synthesis routes described above, specific and non-specific addition. The resultant PEGylated ligands are termed $P100_{SP}$-P4-**1**/**2** and $P100_{NSP}$-P4-**1**/**2**, P4 to indicate the insertion of the PEG4 linker, Table 1. The $P100_{SP}$-P4-**1** and $P100_{SP}$-P4-**2** conjugated peptides were shown to have the expected sizes by gel permeation chromatography (ESI†) and DLS. A further increase of 10 nm in cross-sectional diameter was observed for the addition of the PEG4-fused ligand (Fig. 3B).

An ELISA compared the relative binding affinities of the four PEGylated ligand **2** variants – specific (solid) and non-specific (patterned) attachment with and without the PEG4 linker, Fig. 5A. $P100_{SP}$-**2** demonstrates a higher binding affinity for cell surface PSMA than $P100_{NSP}$-**2**, illustrating the significance of the unmodified Glu sidechain obtained through specific attachment. Furthermore, inclusion of the PEG4 linker further enhances the binding affinity for both $P100_{SP}$-**2** and $P100_{NSP}$-**2**. As a result, the PEGylated ligand $P100_{SP}$-P4-**2** incorporating the PEG4 linker with specific attachment site provided the most effective architecture for the PEGylated ligand to recognize PSMA on the cell surface.

The dual ligand combinations of peptides **1** and **2** were expected to further provide higher affinity through bidentate binding. However, only a modest improvement was observed for the combination of $P100_{NSP}$-**2** + $P100_{NSP}$-**1** *versus* the best individual ligand, $P100_{SP}$-P4-**2**, Fig. 5B. The slightly greater binding affinity can be attributed to the bidentate binding mode of the dual ligand system. Furthermore, the architecture of the PEG4 (P4) linker also required optimization. The geometry of the PEG4 linker clearly affects the availability of the two Lys sidechains in the 8-mer peptide **1**, as shown by the drop in affinity for $P100_{NSP}$-P4-**2** + $P100_{NSP}$-P4-**1**. This reduction in apparent binding affinity could be due to the formation of a crown ether-like cavity by PEG4, which naturally adopts a mushroom-like conformation based on its size.[34] Furthermore, the combination has affinity equivalent to $P100_{NSP}$-P4-**2**, which indicates complete loss of ligand **1** activity by PEG4 masking; this effect renders the dual ligand combination of $P100_{NSP}$-P4-**2** + $P100_{NSP}$-P4-**1** equivalent to the individual ligand, $P100_{NSP}$-P4-**2**. Notably, ligand **2** lacks Lys residues, and is therefore not susceptible to such masking effects.

Controlling the geometry of the PEG4 linker could prevent masking of the Lys sidechains of ligand **1**. Sandwiching PEG4 between PEG100 and the peptide ligand through the specific attachment mode, eliminates such debilitating effects, as shown by a significant increase in binding affinity for the dual ligand system $P100_{SP}$-P4-**2** + $P100_{SP}$-P4-**1** (Fig. 5B and Fig. S9, ESI†). This specific attachment incorporating the PEG4 linker evidently stretches the PEG4 providing higher apparent affinity from a constitutional isomer with different geometry. Thus, in the next experiments, phage were wrapped with the dual ligand combination of $P100_{SP}$-P4-**2** + $P100_{SP}$-P4-**1** in a 2 : 1 ratio.

PEG spacers to control relative ligand spacing

The relative spacing between ligands governs the synergy of the chelate-based avidity effect. To achieve optimal geometry of the two ligands, the relative spacing was systematically engineered by interspersing long PEGylated ligands with smaller PEG wrappers on the phage surface. The smaller PEG wrappers could provide spacers to push apart the PEG-fused ligands on

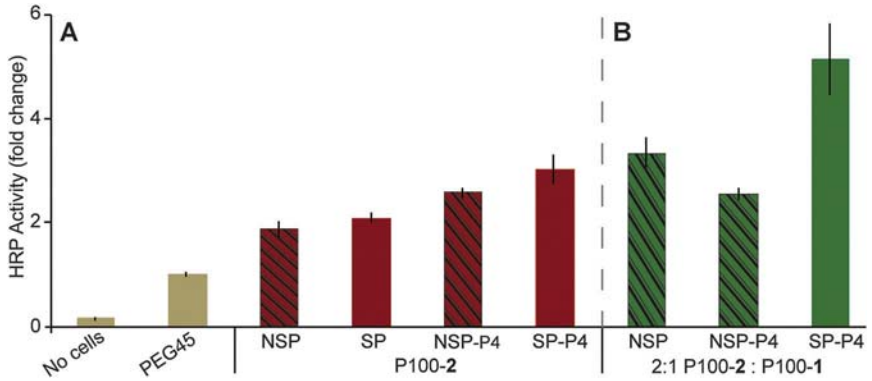

Fig. 5 (A) Phage-based ELISA comparing the different attachment modes with the incorporation of a PEG4 linker for PEGylated ligand **2** (red bars) targeting PSMA on LNCaP cells. Patterned bars indicate non-specific (NSP) attachment modes. (B) The combination of ligands **1** and **2** (green bars) leads to increased affinity due to the chelate-based avidity effect. The p-value is <0.01 for all data reported here.

the phage surface. Generating ligands and spacers required the two wrapping modes described above, click chemistry and cysteine–maleimide reaction, on the same phage. K_{14}-alkyne and K_{14}-Cys were pre-mixed to an estimated mole fraction of 0.19 (as described above), and then used to wrap the phage surface. K_{14}-alkyne was linked to short PEG polymers to provide spacers. Different concentrations of the PEG polymers were explored. The ratio of ligands to spacers was empirically optimized, and a ratio of 1.5 : 1 provided the best levels of PSMA recognition (data not shown). The concentration of the PEGylated ligands remained unchanged, and a 2 : 1 molar mixture of the two ligands was reacted with the K_{14}-Cys wrapped on the phage surface. A higher net concentration of wrappers could be accommodated by the phage as the spacers allowed higher packing density.

The dual PSMA ligand combination described above, $P100_{SP}$-P4-**2** + $P100_{SP}$-P4-**1**, without (green) or with spacers (brown) of either PEG 7, 22 or 45, wrapped around the phage were assayed for binding to LNCaP cells, Fig. 6. All spacers significantly enhanced PSMA recognition by the displayed ligands. However, the PEG7 spacer proved most effective. The much smaller PEG7 spacer can force the ligands into adopting a more optimal geometry for effective bidentate binding, and the height of this polymer brush does not interfere with ligand binding. Longer spacers failed to boost binding affinity to the same levels. At the mole fraction of PEG used, the PEG polymers can adopt the brush conformation with the height of the polymer brush dependent on the PEG length. Interdigitation of PEG spacers with PEGylated ligands can interfere with the binding affinity of the ligands, as shown with the longer brushes of PEG22 and 45. Also, the addition of K_{14}-alkyne without conjugated PEG spacers has no effect on binding affinity, as expected; thus, the increased packing of oligolysine wrappers is not a contributing factor. Rather, enhanced binding results from the improved geometry through addition of PEG spacers.

Selective recognition of PSMA positive cells

To demonstrate specificity for PCa cells by these chemically modified phage, binding to different prostate cancer cell lines was compared. LNCaP cells can model early or late stage cancer

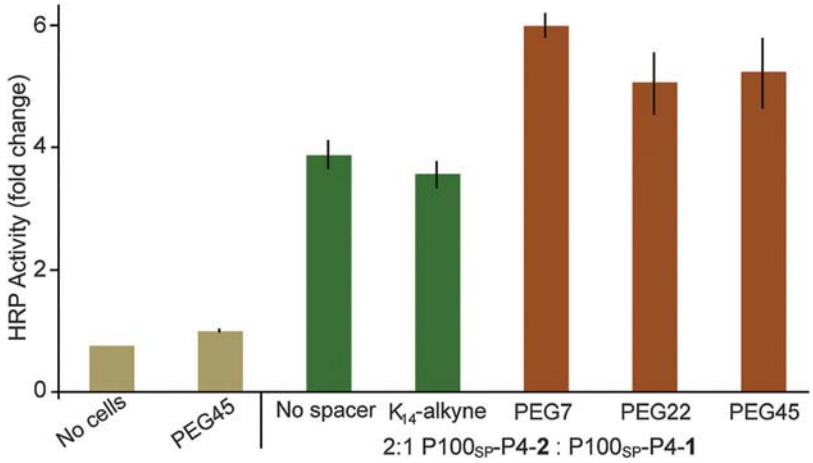

Fig. 6 Phage-based ELISA demonstrates the effect of smaller PEG polymers applied as spacers to optimize the geometry of the PEGylated dual ligand combination of $P100_{SP}$-P4-**2** + $P100_{SP}$-P4-**1**. The dual ligand combination on phage was assayed with (brown) and without (green) PEG spacers. The p-value is <0.01 for all data reported here.

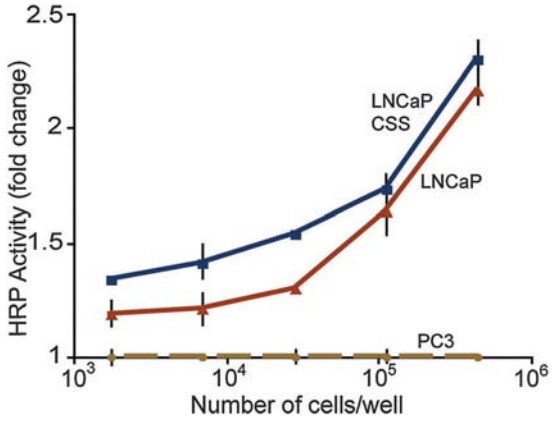

Fig. 7 A dose response curve demonstrates the specificity of PSMA detection on two types of LNCaP cells relative to the PSMA-negative PC3 cells, as shown by cell-based ELISA. The dual ligand combination of $P100_{SP}$-P4-**2** + $P100_{SP}$-P4-**1** and the PEG7 spacer on phage was used for specific detection of PSMA on the cell surface.

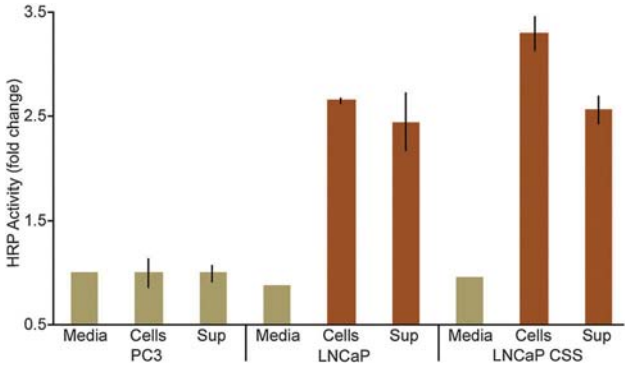

Fig. 8 A sandwich ELISA demonstrating capture of PSMA positive cells by the dual ligand combination of $P100_{SP}$-P4-**2** + $P100_{SP}$-P4-**1** and the PEG7 spacer on phage, which are immobilized on the microtiter plate. Controls are shown in gold color. 'Media' indicates fresh culture media, whereas 'sup' indicates cell culture supernatant. The p-value is <0.01 for all data reported here.

cells, through variation in their culture conditions. The majority of PCa cases gain resistance to therapies based on androgen ablation.[51] The LNCaP cell line, a model for early stage PCa, is androgen sensitive but gradually loses the androgen requirement, providing a model for late stage PCa, which also mimics androgen ablation.[51,52] The latter can be simulated by culturing LNCaP cells in androgen-depleted media, referred to as LNCaP CSS (for charcoal-stripped serum).[53,54] Increased levels of PSMA are associated with androgen independent PCa.[52] Thus, both LNCaP and LNCaP CSS cell lines were assayed. The third cell line, PC3 cells, do not express PSMA, and were used as the negative control.[33,55] The following assays validate the dual ligand system for cell line discrimination and quantification of cell surface receptors.

The optimized dual ligand combination of $P100_{SP}$-P4-**2** + $P100_{SP}$-P4-**1** and the PEG7 spacer was assayed for binding to LNCaP (red), LNCaP CSS (blue), and PC3 cell lines (gold), Fig. 7. The results demonstrate high specificity for PSMA positive LNCaP cells in a dose-dependent manner with higher apparent affinity to LNCaP CSS cells. This higher sensitivity to LNCaP CSS cells is consistent with the increase in PSMA expression resulting from the progression of the cancer cells to an androgen independent state in the LNCaP CSS model.[52]

Detecting PSMA on suspended cells and in culture media

The tailored phage could also capture cells from solution, which is critical for future analytical applications in circulating tumor cell detection and characterization. In this experiment unlike other ELISAs described here, the phage were immobilized on the microtiter plate before applying a solution of cells, Fig. 8 and Fig. S10 (ESI†); levels of bound cells were quantified through application of anti-PSMA primary antibody and HRP-conjugated, anti-mouse, secondary antibody. Again, phage wrapped with the dual ligand combination of $P100_{SP}$-P4-**2** + $P100_{SP}$-P4-**1** and the PEG7 spacer were used. In this experiment, the capture of PSMA positive cells is detected by and proportional to cell surface PSMA concentration. PC3 cells, lacking PSMA, do not generate a significant response, as expected.

PSMA levels are elevated in the urine samples of PCa patients, and levels of this biomarker correlate with the aggressiveness of the disease.[8,56] Therefore, cultured PCa cells should release PSMA into their culture media. Thus, PSMA detection was also performed with cell culture supernatant, normalized to the volume and the number of cells (Fig. 8). The PEGylated dual ligand combination on phage allows sensitive PSMA detection in 100 μL of supernatant from both LNCaP and LNCaP CSS cell cultures. Cell culture media from PC3 cells and fresh culture medias serve as the negative controls. As expected, the negative controls failed to show any significant binding. The effective detection of PSMA shed by LNCaP cells, in androgen sensitive and androgen independent cells, demonstrates the use of phage wrapped with PEGylated ligands for future development of analytical devices and translation to the clinic.

Conclusions

In conclusion, this study demonstrates a systematic approach to engineering the phage surface through chemical tailoring. Chemically modifying viruses with PEG addresses a major issue of non-specific adhesion to cellular surfaces, and further engineering allowed specific detection using PEGylated ligands. The reported PEGylated dual ligand combination provides a foundation for applying the phage to cell-based analysis, where highly specific molecular recognition of cells is essential. Optimization of binding affinity required optimization of the PEG length, packing density, point of attachment, linkers and spacers. The versatility of PEG allows such multivariate optimization. This biocompatible polymer is widely available with diverse functionalities for bioconjugation and also has moderately predictable conformations to guide engineering. Furthermore, we demonstrate control over the relative spatial configuration of the ligands using small PEG polymers interdigitated with larger PEG brushes in a general approach applicable to many binding optimization

studies. Most importantly, these chemically modified phage could readily distinguish PSMA-positive from PSMA-negative cells, and also identify more aggressive PCa tumor cells. In the future, we will apply such phage to the capture and detection of circulating tumor cells for use in cell-based detectors.

Acknowledgements

We gratefully acknowledge support from the NIH through grants from the NAID (1 R43 AI074163) and the NCI (1 R43 CA050779). We thank our long-term collaborator, Prof. Reginald M. Penner, for helpful conversations. Kritika Mohan acknowledges support from the graduate fellowship awarded by the ACS division of Analytical Chemistry, and sponsored by the Society for Analytical Chemists of Pittsburgh (SACP), the Allergan graduate fellowship in synthetic organic chemistry, and the Taihi Hong memorial graduate student education award. We also gratefully acknowledge Dr Beniam Berhane for his helpful suggestions. The approach reported here has been licensed to PhageTech, a company co-founded by Prof. Weiss and Prof. Penner. PhageTech is developing products related to the research described in this paper. The terms of this arrangement have been reviewed and approved by the University of California, Irvine in accordance with its conflict of interest policies.

Notes and references

1 S. A. Joosse, T. M. Gorges and K. Pantel, *EMBO Mol. Med.*, 2015, **7**, 1–11.
2 P. Mehlen and A. Puisieux, *Nat. Rev. Cancer*, 2006, **6**, 449–458.
3 R. L. Siegel, K. D. Miller and A. Jemal, *Ca-Cancer J. Clin.*, 2015, **65**, 5–29.
4 K. Mohan, K. C. Donavan, J. A. Arter, R. M. Penner and G. A. Weiss, *J. Am. Chem. Soc.*, 2013, **135**, 7761–7767.
5 N. Schülke, O. A. Varlamova, G. P. Donovan, D. Ma, J. P. Gardner, D. M. Morrissey, R. R. Arrigale, C. Zhan, A. J. Chodera, K. G. Surowitz, P. J. Maddon, W. D. W. Heston and W. C. Olson, *Proc. Natl. Acad. Sci. U. S. A.*, 2003, **100**, 12590–12595.
6 A.-Y. Chuang, A. M. DeMarzo, R. W. Veltri, R. B. Sharma, C. J. Bieberich and J. I. Epstein, *Am. J. Surg. Pathol.*, 2007, **31**, 1246–1255.
7 M. Kawakami and J. Nakayama, *Cancer Res.*, 1997, **57**, 2321–2324.
8 R. L. Sokoloff, K. C. Norton, C. L. Gasior, K. M. Marker and L. S. Grauer, *Prostate*, 2000, **43**, 150–157.
9 K. Mohan and G. A. Weiss, *Anal. Biochem.*, 2014, **453**, 1–3.
10 J. A. Arter, J. E. Diaz, K. C. Donavan, T. Yuan, R. M. Penner and G. A. Weiss, *Anal. Chem.*, 2012, **84**, 2776–2783.
11 G. P. Smith, *Science*, 1985, **228**, 1315–1317.
12 S. S. Sidhu and G. A. Weiss, *Phage Display: A Practical Approach*, Oxford University Press, New York, 2004.
13 J. K. Scott and G. P. Smith, *Science*, 1990, **249**, 386–390.
14 L. C. Welsh, M. F. Symmons, J. M. Sturtevant, D. A. Marvin and R. N. Perham, *J. Mol. Biol.*, 1998, **283**, 155–177.
15 M. Trepel, W. Arap and R. Pasqualini, *Curr. Opin. Chem. Biol.*, 2002, **6**, 399–404.
16 G. Abbineni, S. Modali, B. Safiejko-Mroczka, V. A. Petrenko and C. Mao, *Mol. Pharmaceutics*, 2010, **7**, 1629–1642.
17 W. Arap, R. Pasqualini and E. Ruoslahti, *Science*, 1998, **279**, 377–380.
18 K. Ma, D.-D. Wang, Y. Lin, J. Wang, V. Petrenko and C. Mao, *Adv. Funct. Mater.*, 2013, **23**, 1172–1181.
19 Y. Wang, Z. Ju, B. Cao, X. Gao, Y. Zhu, P. Qiu, H. Xu, P. Pan, H. Bao, L. Wang and C. Mao, *ACS Nano*, 2015, **9**, 4475–4483.
20 V. A. Petrenko and P. K. Jayanna, *FEBS Lett.*, 2014, **588**, 341–349.
21 P. K. Jayanna, V. P. Torchilin and V. A. Petrenko, *Nanomedicine*, 2009, **5**, 83–89.
22 T. Wang, S. Yang, V. A. Petrenko and V. P. Torchilin, *Mol. Pharmaceutics*, 2010, **7**, 1149–1158.
23 P. Ngweniform, G. Abbineni, B. Cao and C. Mao, *Small*, 2009, **5**, 1963–1969.
24 S. Kalarical Janardhanan, S. Narayan, G. Abbineni, A. Hayhurst and C. Mao, *Mol. Cancer Ther.*, 2010, **9**, 2524–2535.
25 D. Ghosh, Y. Lee, S. Thomas, A. G. Kohli, D. S. Yun, A. M. Belcher and K. A. Kelly, *Nat. Nanotechnol.*, 2012, **7**, 677–682.
26 D. Ghosh, A. F. Bagley, Y. J. Na, M. J. Birrer, S. N. Bhatia and A. M. Belcher, *Proc. Natl. Acad. Sci. U. S. A.*, 2014, **111**, 13948–13953.
27 Z. M. Carrico, M. E. Farkas, Y. Zhou, S. C. Hsiao, J. D. Marks, H. Chokhawala, D. S. Clark and M. B. Francis, *ACS Nano*, 2012, **6**, 6675–6680.
28 M. Russel, H. B. Lowman and C. Tim, *Phage Display: Practical Approach*, Oxford University Press, New York, 2004.
29 J. A. Lamboy, P. Y. Tam, L. S. Lee, P. J. Jackson, S. K. Avrantinis, H. J. Lee, R. M. Corn and G. A. Weiss, *ChemBioChem*, 2008, **9**, 2846–2852.
30 J. A. Lamboy, J. A. Arter, K. A. Knopp, D. Der, C. M. Overstreet, E. F. Palermo, H. Urakami, T.-B. Yu, O. Tezgel, G. N. Tew, Z. Guan, K. Kuroda and G. A. Weiss, *J. Am. Chem. Soc.*, 2009, **131**, 16454–16460.
31 M. G. Dozmorov, R. E. Hurst, D. J. Culkin, B. P. Kropp, M. B. Frank, J. Osban, T. M. Penning and H.-K. Lin, *Prostate*, 2009, **69**, 1077–1079.
32 J. S. Horoszewicz, S. S. Leong, T. M. Chu, Z. L. Wajsman, M. Friedman, L. Papsidero, U. Kim, L. S. Chai, S. Kakati, S. K. Arya and A. A. Sandberg, *Prog. Clin. Biol. Res.*, 1980, **37**, 115–132.
33 R. E. Sobel and M. D. Sadar, *J. Urol.*, 2005, **173**, 342–359.
34 D. Marsh, R. Bartucci and L. Sportelli, *Biochim. Biophys. Acta, Biomembr.*, 2003, **1615**, 33–59.
35 J. Crawford, *Cancer Treat. Rev.*, 2002, **28**, 7–11.
36 K. Knop, R. Hoogenboom, D. Fischer and U. S. Schubert, *Angew. Chem., Int. Ed. Engl.*, 2010, **49**, 6288–6308.
37 S. S. Pai, T. M. Przybycien and R. D. Tilton, *Langmuir*, 2010, **26**, 18231–18238.
38 C. S. Fishburn, *J. Pharm. Sci.*, 2008, **97**, 4167–4183.
39 C. Loo, A. Lin, L. Hirsch, M.-H. Lee, J. Barton, N. Halas, J. West and R. Drezek, *Technol. Cancer Res. Treat.*, 2004, **3**, 33–40.

40 C. Loo, A. Lowery, N. Halas, J. West and R. Drezek, *Nano Lett.*, 2005, **5**, 709–711.
41 C. S. Levin, S. W. Bishnoi, N. K. Grady and N. J. Halas, *Anal. Chem.*, 2006, **78**, 3277–3281.
42 X. Xia, M. Yang, Y. Wang, Y. Zheng, Q. Li, J. Chen and Y. Xia, *ACS Nano*, 2012, **6**, 512–522.
43 M. Sarma, T. Chatterjee and S. K. Das, *RSC Adv.*, 2012, **2**, 3920–3926.
44 R. B. Greenwald, Y. H. Choe, J. McGuire and C. D. Conover, *Adv. Drug Delivery Rev.*, 2003, **55**, 217–250.
45 G. Montesano, R. Bartucci, S. Belsito, D. Marsh and L. Sportelli, *Biophys. J.*, 2001, **80**, 1372–13783.
46 M. J. Glucksman, S. Bhattacharjee and L. Makowski, *J. Mol. Biol.*, 1992, **226**, 455–470.
47 J. Kim, N. Korkmaz and C. H. Nam, *Interdiscip. Bio Cent.*, 2012, **4**, 1–7.
48 Y. Liu, M. K. Shipton, J. Ryan, E. D. Kaufman, S. Franzen and D. L. Feldheim, *Anal. Chem.*, 2007, **79**, 2221–2229.
49 J. Manson, D. Kumar, B. J. Meenan and D. Dixon, *Gold Bull.*, 2011, **44**, 99–105.
50 J. M. Harris, N. E. Martin and M. Modi, *Clin. Pharmacokinet.*, 2001, **40**, 539–551.
51 C. Tovar, B. Higgins, K. Kolinsky, M. Xia, K. Packman, D. C. Heimbrook and L. T. Vassilev, *Mol. Cancer*, 2011, **10**, 49–59.
52 S. R. Denmeade, L. J. Sokoll, S. Dalrymple, D. M. Rosen, A. M. Gady, D. Bruzek, R. M. Ricklis and J. T. Isaacs, *Prostate*, 2003, **54**, 249–257.
53 Z. Culig, J. Hoffmann, M. Erdel, I. E. Eder, A. Hobisch, A. Hittmair, G. Bartsch, G. Utermann, M. R. Schneider, K. Parczyk and H. Klocker, *Br. J. Cancer*, 1999, **81**, 242–251.
54 Y. Iwasa, A. Mizokami, S. Miwa, K. Koshida and M. Namiki, *Int. J. Urol.*, 2007, **14**, 233–239.
55 A. Ghosh, X. Wang, E. Klein and W. D. W. Heston, *Cancer Res.*, 2005, **65**, 727–731.
56 S. L. Su, I. P. Huang, W. R. Fair, C. T. Powell and W. D. Heston, *Cancer Res.*, 1995, **55**, 1441–1443.